# Broken Rotor Bar Fault Detection and Severity Identification in Squirrel Cage Induction Motor Using Empirical Mode Decomposition and Artificial Neural Networks

**Dimas Anton Asfani**
Department of Electrical Engineering, Institut Teknologi Sepuluh Nopember, Indonesia
da.asfani@its.ac.id (corresponding author)

**Muhammad Lucky Hari Andono**
Department of Electrical Engineering, Institut Teknologi Sepuluh Nopember, Indonesia
luckyandono@gmail.com

**Daniar Fahmi**
Department of Electrical Engineering, Institut Teknologi Sepuluh Nopember, Indonesia
daniarfahmi@ee.its.ac.id

**I. Gusti Ngurah Satriyadi Hernanda**
Department of Electrical Engineering, Institut Teknologi Sepuluh Nopember, Indonesia
didit@ee.its.ac.id

**I. Made Yulistya Negara**
Department of Electrical Engineering, Institut Teknologi Sepuluh Nopember, Indonesia
yulistya@ee.its.ac.id

*Received: 2 April 2025 | Revised: 13 May 2025 | Accepted: 24 May 2025*

 *DOI: https://doi.org/10.48084/etasr.11259*

**ABSTRACT**

**The broken rotor bar is the fault that most often occurs in induction motors. This paper proposes a method to identify the broken rotor bar fault using a combination of Empirical Mode Decomposition and Artificial Neural Networks (ANNs). The motor current signal is processed using EMD analysis resulting in the Intrinsic Mode Function (IMF) signal. The zero crossing point of the IMF signal is recorded to obtain the Time Successive between Zero Crossing (TSZC). The Probability Density Function (PDF) of the TZSC is used as the ANN classifier input. The PDF properties of peak, width, and standard deviation are selected as the input variables. Two ANNs were designed as fault detection and severity identification systems. The experimental testing also considers the load level variation. The experiment of the broken rotor bar fault diagnostics shows that the ANN-based fault detection system is able to detect faults with accuracy up to 94.2%. Moreover, the ANN-based severity identification successfully identified 76.09% of the cases. In addition, the experiment on load variations reveals that the fault diagnostic is more effective at higher loads.**

***Keywords-induction motor; empirical mode decomposition; intrinsic mode function; probability density function; artificial neural networks***

## I. INTRODUCTION

Three-phase induction motors are a type of electric machine widely used in industry because of their reliability and simplicity in construction, especially squirrel-cage induction motors [1]. Compared with the wound rotor type, the lack of a brush and slip ring means that the squirrel-cage induction motors are better in terms of efficiency and maintenance. Moreover, their capital and maintenance costs are relatively lower compared to other electric machines. However, despite

their reliability, squirrel-cage induction motors are also known for several faults that initiate from operating, thermal, electrical, mechanical, and environmental stress. Because of their important role in industry, faults inside induction motors may have a significant impact on the production process, high cost of repairs, and production losses [2]. The incipient fault should be detected and solved as soon as possible to avoid catastrophic failure and the initiation of damage to other parts of the motor [3]. The BRB may bend outside of the rotor. Considering the small size of the airgap, the broken part can contact the stator teeth, causing damage. This can generate eccentricity and reduce the operating lifetime of the motor not only on the stator side, but also on the rotor side [4].

Several methods have been used to detect BRBs in squirrel-cage induction motors, such as machine learning [5], analysis of the d-q plan [6], residual shrinkage network [7], frequency analysis of multi-sensor systems [8], and adaptive window short-time Esprit [9]. In addition to these methods, Motor Current Signature Analysis (MCSA), a method based on the frequency analysis of the motor current signal, is commonly deployed. This method is used in practice and is continuously being developed because of its simplicity and capability to detect common faults in electric machines, especially BRBs [10].

ANNs, which can be used as classifier methods, are suitable for identifying BRBs. The combination of variable measurement, signal processing, and ANN is an interesting approach to provide the most effective fault detection system [11]. Some options for the measurement of variables include motor current [12], acoustic [13], vibration [14], and flux [15]. The optimal design of the ANN, including the architecture, training method, input variable selection, and output definition, is a challenge for improving performance and efficiency [16].

This study proposes a method for diagnosing induction motors, particularly for detecting BRB faults. The faults were detected by performing EMD analysis of the stator current. Through the EMD analysis, the stator current was decomposed into waveforms of IMF. The TSZC of the IMF waveform was then extracted to obtain the detection variable. For accurate classification, this study employed an ANN to detect the existence of faults and their severity.

## II. COMBINATION OF EMD AND ANN FOR MOTOR DIAGNOSTIC

In this section, EMD analysis is explained step-by-step. Moreover, the ANN employed in this research is also explained briefly.

### *A. Empirical Mode Decomposition*

In order to decompose the motor supply current waveform, EMD analysis was employed. This method was chosen for its capability to decompose stationary signals, and therefore, it is suitable for the current decomposition of the stator. A stationary signal is one whose frequency changes with respect to time. The signal is decomposed into several simpler signals called IMFs and one residual signal [1]. Figure 1 shows an example of a signal *x(s)* that is decomposed using the EMD method.

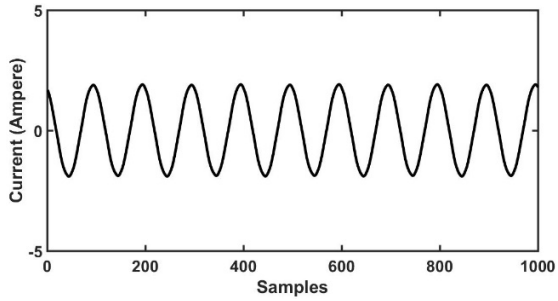


Fig. 1. Original current signal to be decomposed.

In order to get the IMF of the *x(s)* signal, the first step is to look for points of local extrema, which are local maxima and local minima (Figure 2). The *t* of the local extrema is located where the first derivative of the signal is zero:

$$\frac{dx(s)}{ds} = 0 \quad (1)$$

where *s* denotes the number of samples. To determine whether the point is a local maximum or minimum, the second derivative test is needed. For example, if $d^2x(s)/s^2$ is negative, then the point is a local maximum.

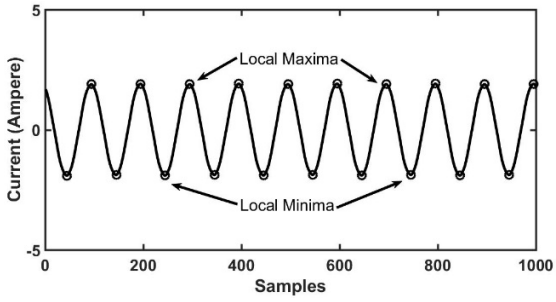


Fig. 2. Local extrema.

The next step is to connect the points of local extrema using cubic spline interpolation to form the Upper Envelope (*UE*). The interpolation function, $B_0(x)$ is defined by (2), where $h = x_{k+1} - x_k = \frac{x_N - x_0}{N}$ [11]. The same procedure was applied to the local minima points to obtain the Lower Envelope (*LE*), as depicted in Figure 3.

$$f(x) = \begin{cases} 0 & , x < 0 \\ \frac{1}{6}\left(2h + (x - x_0)\right)^3 & , x < 0 \\ \frac{2h^3}{3} - \frac{1}{2}(x - x_0)^2\left(2h + (x - x_0)\right), & x < 0 \\ \frac{2h^3}{3} - \frac{1}{2}(x - x_0)^2\left(2h - (x - x_0)\right), & x < 0 \\ \frac{1}{6}\left(2h - (x - x_0)\right)^3 & , x < 0 \\ 0 & , x \geq 0 \end{cases} \quad (2)$$

The mean value of both envelopes is called $m_1$ and is calculated by:

$$m_1 = \frac{UE + LE}{2} \quad (3)$$

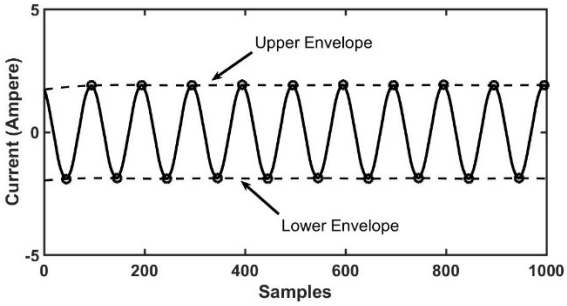


Fig. 3. Upper and lower envelopes.

By subtracting $m_1$ from the original signal, the value of $h_1$ (the first IMF) is obtained. Figure 4 displays the result of subtraction between the original signal and $m_1$.

$$h_1 = x(s) - m_1 \quad (4)$$

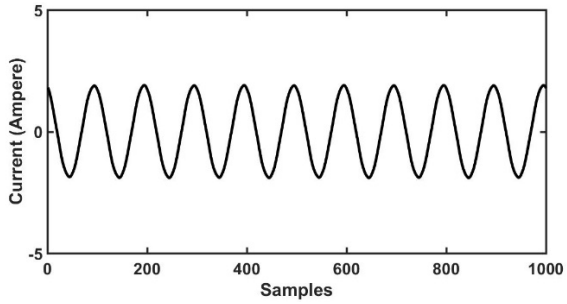


Fig. 4. The signal of the first IMF, $h_1$

$h_1$ is the first IMF, if the following conditions are fulfilled [1]. First, the number of local extrema and zero crossings must be the same or differ at most by one. Second, the mean value of each envelope must be zero. Third, the number of iterations for searching the IMF is limited by the SD between two consecutive *h* values, which is around 0.2 and 0.3.

If $h_1$ does not fulfill these conditions, then the next step is to treat $h_1$ as the main signal, so that $h_1$ will undergo the process of finding the envelope until obtaining the new subtraction between the main signal $h_1$ and newly obtained mean value of the two envelopes, $m_{11}$. This subtraction is now called $h_{11}$.

$$h_{11} = h_1 - m_{11} \quad (5)$$

This process is repeated for as many as *k* iterations until the SD between two consecutive *h* reaches a certain value. After that, the last value of *h* is called $c_1$ and it becomes the first IMF. The first IMF of the EMD decomposed signal is shown in Figure 5. The SD is calculated as:

$$SD = \sum_{t=0}^{T} \left[ \frac{(h_{1(k-1)}(t) - h_{1k}(t)^2}{h_{1(k-1)}^2(t)} \right] \quad (6)$$

The value of $c_1$ is expressed considering the target of *k*-iteration:

$$c_1 = h_{1k} \quad (7)$$

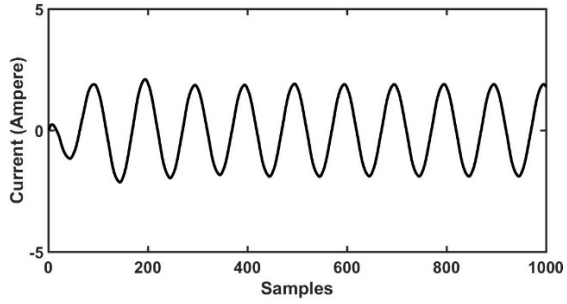


Fig. 5. Signal of IMF 1.

After obtaining the value of the first IMF, the next step is to subtract the original signal from the first IMF to obtain the residual signal. The residual signal $r_1$ is calculated by:

$$r_1 = x(s) - c_1 \quad (8)$$

The next IMF can be extracted from the residual signal $r_1$ as long as it is not a monotonic function, which still has several local maxima and local minima. The following step is to treat $r_1$ as the main signal and the process of obtaining IMF is repeated until the SD value between new consecutive $h_1$ has been met; then the value of the last *h* is called $c_2$ and in other words, IMF 2. The iterations are performed continuously until the residual signal becomes a monotonic function. The original signal can be reconstructed by adding the residual signal to all the extracted IMF. The EMD results are illustrated in Figure 6. The original signal *x(s)* can be reconstructed by summing all the IMF signals:

$$x(s) = \sum_{i=1}^{n} c_i + r \quad (9)$$

where $c_i$ is the IMF signal and *r* is the residual signal.

The EMD analysis is a deterministic method with subsequent calculations. Similar to the Fast Fourier Transform (FFT), which is widely used in commercial products, EMD analysis is feasible for industrial applications.

### *B. Artificial Neural Networks*

There are several types of ANN architectures, such as Feed-Forward Networks (FFNN), backpropagation, recurrent networks, feedback networks, radial basis function networks, and Kohonen self-organizing map networks. Of all these types, FFNN is the most widely used because of its simple architecture, ability to be applied as a classifier, and low computational load [17]. Moreover, the Convolutional Neural Network (CNN) provides another option when the input variables are considered image data, such as the Continuous Wavelet Transform (CWT) [11].

The proposed method uses a multilayer neural network with three variable inputs from the EMD analysis of the motor current signal. The output of the network is a numerical value representing the motor operation condition, which consists of normal, BRB fault, and severity conditions.

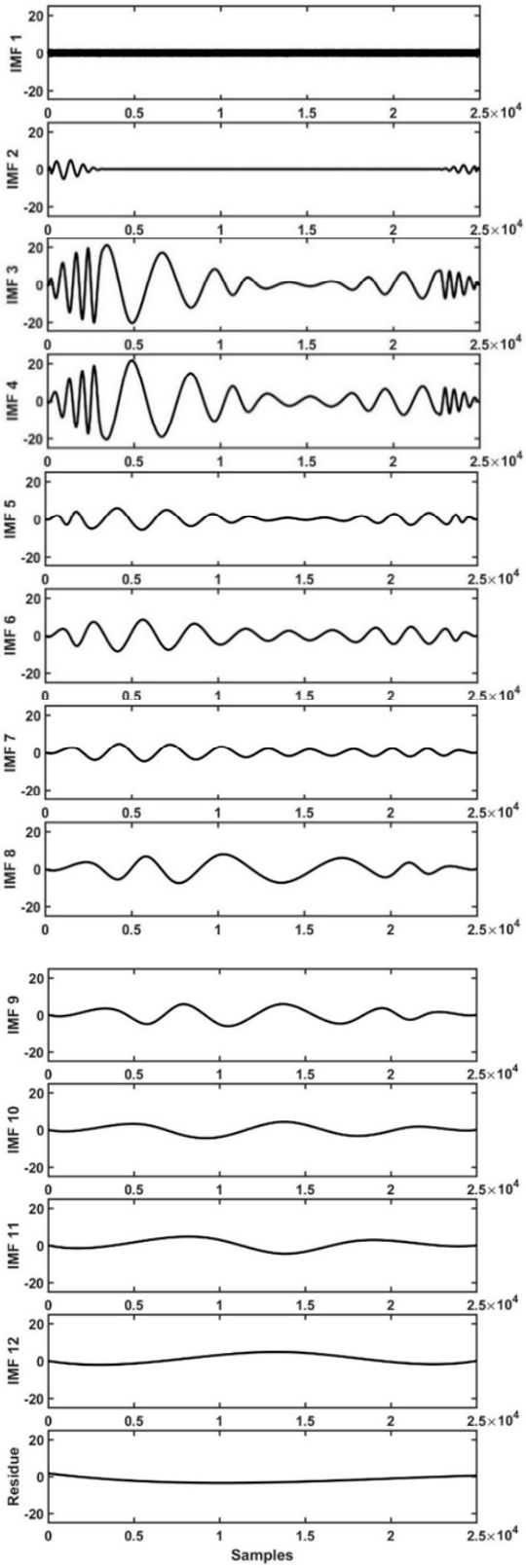


Fig. 6. The results of EMD analysis.

## III. EXPERIMENTAL SETUP

This study employed EMD analysis with an ANN as the classifier. The measurement was conducted at the current that supplies the motor's stator. The system used in this study consisted of an induction motor, a synchronous generator as the motor load, a Data Acquisition (DAQ) system, several measuring devices, and a list software program. The overall system is shown in Figure 7.

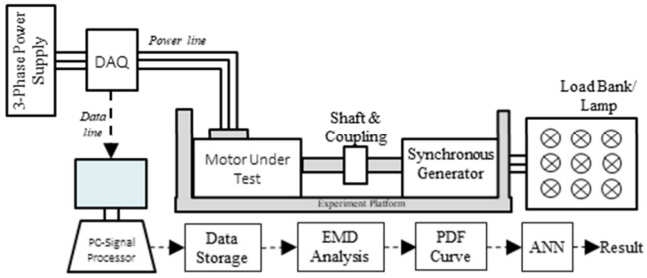


Fig. 7. Experimental scheme

### *A. System Configuration*

The induction motor used in this study was a 2 HP, 3-Phase, 380 V, and 0.6 A. A synchronous generator was used as the mechanical load for the motor and coupled with the rotor of the induction motor. To vary the load, the generator was connected to various numbers of 100-Watt lamps with switches. The current signal was recorded using a DAQ at 5 kS/s for 5 s, resulting in 25000 data points. Each case was recorded 25 times. Therefore, each sampling case consisted of 25 signals, each with 25000 data points.

### *B. Broken Rotor Bar Simulation and Motor Load*

The condition of the BRB in this study was modeled by a hole in the rotor bar. There were four variations in the bar conditions: 1 BRB (1 hole on the rotor bar), 2 BRB (2 holes), 3 BRB (3 holes), and 8 BRB (8 holes) (Figure 8). The holes in the rotor bar were created by drilling the rotor bar to a specific depth. Each BRB hole had a depth of 3 mm by 7 mm (Figure 9).

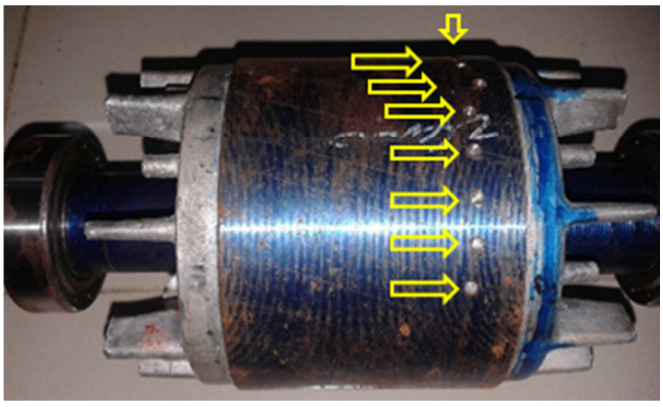

Fig. 8. The 8 BRB rotor.

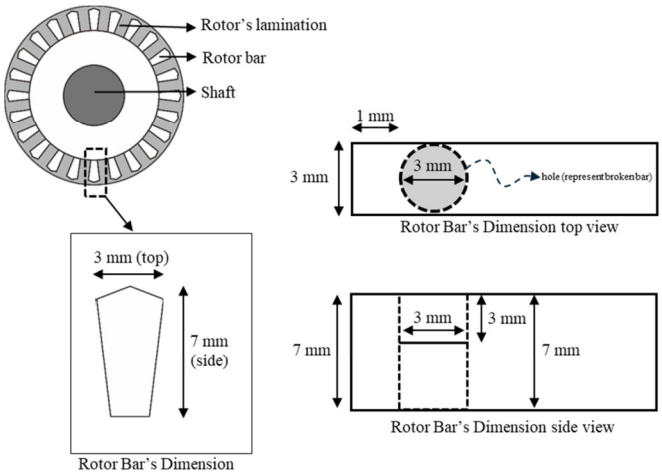


Fig. 9. Diagram of the rotor with a BRB scheme.

The loading condition was specified to be 900 Watt or equal to nine lamps for the maximum load. The electrical load on the synchronous generator was gradually increased. The initial condition given to the motor was the No Load condition. On the next condition, the motor was coupled with a synchronous generator, but the generator itself was not loaded at all, so the motor's load was the pure generator's inertia. Subsequently, the generator was gradually loaded by a lamp as a mechanical load for the induction motor. The electrical loads for the generator were 300 W (3 lamps), 600 W (6 lamps), and 900 W (9 lamps).

### *C. Signal Processing*

The first step in signal processing involves calculating the IMF of the steady-state motor current signal. The next step is to find the zero crossings of the IMF. The sample between the two consecutive zero crossings is recorded as Sample Between Zero Crossing (SBZC). The time or duration of SBZC was calculated as the TSZC. The IMF considered in the fault diagnostic process is the one having a TSZC of around half cycle of the power frequency [1]. In this study, the IMF used was the one with a TSZC of approximately 10 ms, with an SBZC value of 50 samples, and with a power supply of 50 Hz.

### *D. Bearing Fault Classification based on ANN*

The architecture of an ANN is defined based on the data characteristics or problem dependency. Heuristic approaches and simulation result analyses are typically used for the initial selection of the number of hidden layers and nodes [18]. Based on the initial selection and scanning of the hidden layer and node, the defined ANN architecture consists of one input layer, two hidden layers, and one output layer. The number of hidden layers was optimized by systematic searching within a specific range and was selected from 21 to 30 nodes [19]. Each combination was trained ten times to obtain the best training performance. Two ANNs were proposed for this method. The first ANN was designed to distinguish between normal and BRBs, and the second was designed to identify the severity level of the fault. The FFNN was selected because of its simple architecture and pattern recognition capability. The ANN configuration is described in detail in Table I.

TABLE I. ANN CONFIGURATION

| ANN specifications | FFNN |
|---|---|
| Learning function | Levenberg-Marquardt algorithm |
| Input layer | 3 nodes or 3 variable input |
| Number of hidden layers | 2 |
| Activation function<br>Hidden layer -1 and 2 | Tansig or hyperbolic tangent sigmoid function |
| Output layer | 1 node or single output |
| Activation function output layer | Pureline or liniear function |
| Dataset | 70% of data for training<br>15% of data for validation<br>15% of data for testing |

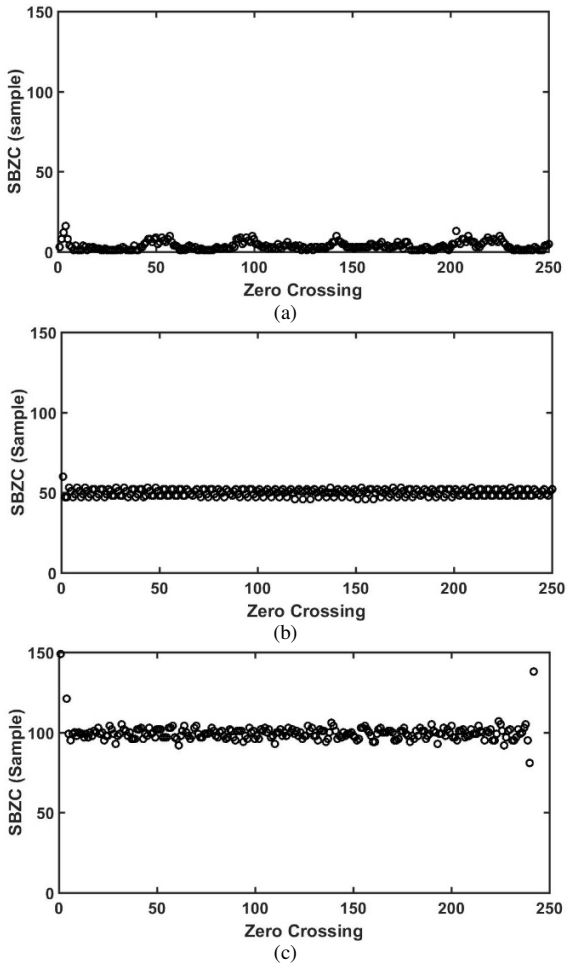


Fig. 10. The SBZC from (a) IMF 1, (b) IMF 2, and (c) IMF 3 obtained from the signal of normal operation.

## IV. RESULTS AND DISCUSSION

The steady-state motor current was recorded using a DAQ system. The current signal was then processed utilizing EMD to obtain a variable input for the ANN-based detection system.

### *A. Broken Rotor Detection System using EMD Analysis*

The two categories of motor conditions used represent normal and BRB faults. The current signal was processed deploying EMD to understand the characteristics of the signal. Figures 10 and 11 show the typical results for the normal and fault conditions after the EMD process, respectively. Normal

and BRB fault operations are easily distinguished by the pattern of the SBZC of IMF 3, as displayed in Figures 10c and 11c.

The next process is the conversion from SBZC to TSZC by multiplying with the time sampling of 0.2 ms and then calculating the TSZC standard deviation. Figure 12a presents a comparison of the SD trend between normal and fault operations, whereas Figure 12b demonstrates the PDF of both operations. From the PDF, it is easier to distinguish the fault operation based on the shape of the curve, especially the peak and width. More details regarding the parameter detection for identifying faults are provided in Figure 13. Three parameters were used as identification parameters and as input variables for the ANN detection system: the peak value, modus, and SD of the PDF curve.

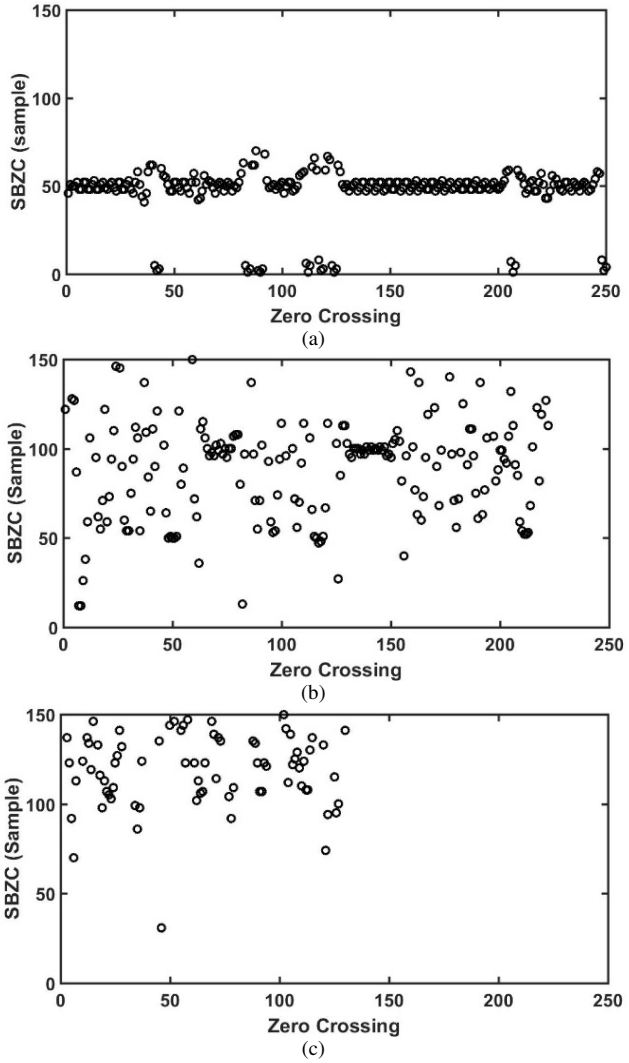


Fig. 11. The SBZC from (a) IMF 1, (b) IMF 2, and (c) IMF 3 obtained from the signal of the BRB fault.

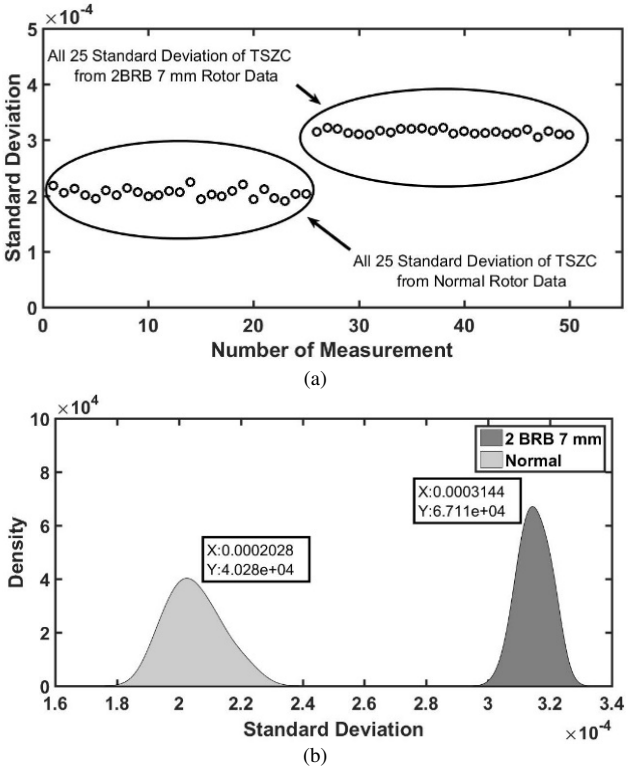


Fig. 12. Comparison of (a) SD and (b) PDF between normal and rotor with 2 BRB 7 mm.

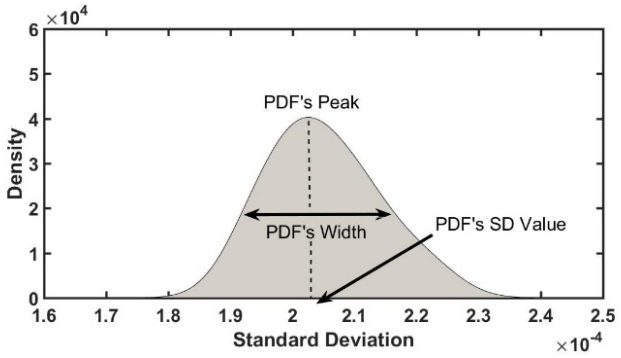


Fig. 13. The PDF dimensions used as input for the ANN.

### *B. ANN Testing to Detect Broken Rotor Bar*

The fault types considered in this case consisted of variations in the number of BRBs, hole depth, and motor loading. The number of BRBs varied by 1, 2, 3 and 8 bars. The depth of the hole was 3 or 7 mm, whereas the motor loading varied from no load, 300 Watt, 600 W, and 900 W. The loading conditions were categorized as low (no load, generator only load, and 300 Watt generator load) and high (600 Watt and 900 Watt generator load).

The detection system target was designed to identify normal or fault operation. The test was performed gradually from the worst fault of 8 BRBs to the light fault of 1 BRB. Targets that are given for all testing by two categories, 0 and 10, for normal and fault, respectively. The tolerance for both

targets was 5, so the output value of the ANN between the numbers 0 and 5 was recognized as a normal condition; otherwise, it was a fault condition. The test results are presented in Tables II–IV. Table II lists the results of the overall/all cases for both low- and high-load operations.

TABLE II. RESULTS OF ANN'S FAULT DETECTION FOR ALL LOADING CATEGORIES

| Condition | Amount of data | Error | Efficiency |
|---|---|---|---|
| 8BRB | 120 | 12 | 90.00% |
| 8BRB+3BRB7 | 180 | 16 | 91.11% |
| 8BRB+3BRB7+3BRB3 | 240 | 23 | 90.42% |
| 8BRB+3BRB7+3BRB3+2BRB7 | 300 | 31 | 89.67% |
| 8BRB+3BRB7+3BRB3+2BRB7+2 BRB3 | 360 | 38 | 89.44% |
| 8BRB+3BRB7+3BRB3+2BRB7+2 BRB3+1BRB7 | 420 | 33 | 92.14% |
| 8BRB+3BRB7+3BRB3+2BRB7+2 BRB3+1BRB7+1BRB3 | 480 | 35 | 92.71% |

TABLE III. RESULTS OF ANN'S FAULT DETECTION FOR LOWER LOAD CONDITION

| Condition | Amount of data | Error | Efficiency |
|---|---|---|---|
| 8BRB | 72 | 10 | 86.11% |
| 8BRB+3BRB7 | 108 | 14 | 87.04% |
| 8BRB+3BRB7+3BRB3 | 144 | 19 | 86.81% |
| 8BRB+3BRB7+3BRB3+2BRB7 | 180 | 24 | 86.67% |
| 8BRB+3BRB7+3BRB3+2BRB7+2 BRB3 | 216 | 30 | 86.11% |
| 8BRB+3BRB7+3BRB3+2BRB7+2 BRB3+1BRB7 | 252 | 23 | 90.87% |
| 8BRB+3BRB7+3BRB3+2BRB7+2 BRB3+1BRB7+1BRB3 | 288 | 21 | 92.71% |

TABLE IV. RESULTS OF ANN'S FAULT DETECTION FOR HIGHER LOAD CONDITION

| Condition | Amount of data | Error | Efficiency |
|---|---|---|---|
| 8BRB | 48 | 2 | 95.83% |
| 8BRB+3BRB7 | 72 | 2 | 97.22% |
| 8BRB+3BRB7+3BRB3 | 96 | 4 | 95.83% |
| 8BRB+3BRB7+3BRB3+2BRB7 | 120 | 7 | 94.17% |
| 8BRB+3BRB7+3BRB3+2BRB7+2 BRB3 | 144 | 8 | 94.44% |
| 8BRB+3BRB7+3BRB3+2BRB7+2 BRB3+1BRB7 | 168 | 10 | 94.05% |
| 8BRB+3BRB7+3BRB3+2BRB7+2 BRB3+1BRB7+1BRB3 | 192 | 14 | 92.71% |

Table II shows that the highest, lowest, and average efficiencies of the ANN for all motor loads were 92.71%, 89.44%, and 90.78 %, respectively. According to Table III, the ANN at a low load had the highest efficiency of 92.71%, the lowest efficiency of 86.11%, and an average efficiency of 88.04%. As demonstrated in Table IV, the ANN with a high motor load had the highest efficiency of 97.22%, lowest of 92.71%, and an average of 94.89%. In this case, the efficiency of the ANN with a higher load was better than that with a lower load. The PDF parameters at a low rotor load were nearly equal to those under the no-load condition. The motor current in the rotor was not high at lower loads. Therefore, its effect on the stator current was negligible. Hence, the ANN at higher loads exhibited a higher efficiency than that at lower loading conditions.

### *C. ANN Testing to Determine Rotor's Severity Degree*

The second ANN system was designed to determine the severity of the fault by categorizing it based on the number of BRBs. The ANN was also tested considering a load level that was divided into lower and higher loading conditions, similar to the first ANN system. The testing scenario was designed gradually to observe the effect of the number of fault variations.

The targets for each test were different. For the ANN with normal and eight BRB data, the values of the target were the same as those in the previous test, that is, 0 and 10 for normal and 8 BRB faults, respectively. For the normal rotor, 8 BRB, and 3 BRB data, the targets were 0 for normal rotor, 10 for 3 BRB, and 20 to 8 BRB, respectively. The other tests were performed using this scheme. The test results are presented in Tables V and VI.

TABLE V. RESULTS OF ANN'S FAULT SEVERITY IDENTIFICATION FOR LOWER LOADING CONDITION

| Condition | Amount of data | Error | Efficiency |
|---|---|---|---|
| 8BRB | 72 | 10 | 86.11% |
| 8BRB+3BRB | 144 | 30 | 79.17% |
| 8BRB+3BRB+2BRB | 216 | 73 | 66.20% |
| 8BRB+3BRB+2BRB+1BRB | 288 | 130 | 54.86% |

TABLE VI. THE RESULTS OF ANN'S FAULT SEVERITY IDENTIFICATION FOR HIGHER LOADING CONDITION

| Condition | Amount of data | Error | Efficiency |
|---|---|---|---|
| 8BRB | 48 | 2 | 95.83% |
| 8BRB+3BRB | 96 | 15 | 84.38% |
| 8BRB+3BRB+2BRB | 144 | 53 | 63.19% |
| 8BRB+3BRB+2BRB+1BRB | 192 | 75 | 60.94% |

Table V shows that the identification of the fault severity by the ANN for the lower loading category was as high as 86.11%. The lowest identification rate was 54.86%, with an average identification rate of 71.89%. The identification performance for the higher loading category is shown in Table VI. The best performance achieved was 95.83%, whereas the lowest was 60.94%, with an average of approximately 76.09%. A comparison between Tables V and VI exhibits that the ANN performed better in the higher loading category in terms of identifying fault severity.

The proposed method is compared to those of similar works. Table VII displays a comparison of the proposed method with those of other related studies, which are based on different signal input variables, data processing, and detection methods. The performance metrics presented in Table VII indicate that the efficiency of the proposed model is competitive with other related studies, but it may not be the highest-ranking in terms of overall performance. Nevertheless, the proposed approach contributes significantly to the field by introducing an alternative analytical framework for evaluating fault severity.

TABLE VII. COMPARISON WITH OTHER WORKS

| Method | Input signal | Data processing and detection system | Efficiency (%) | Comments |
|---|---|---|---|---|
| FFT analysis of vibration signal [14] | Vibration | FFT and machine learning model | 93.2 | Industrial data set |
| Wavelet transform of the current signal [20] | Current signal | Wavelet transform and ANN | 98.8 | Load level variation |
| Side band frequency analysis of flux signal [15] | Flux signal | FFT and side band frequency analysis | N/A | More sensitive than convensional MCSA and vibration analysis |
| Proposed method | Electrical current signal | EMD and ANN | 92.7 | Able to predict severity |

## V. CONCLUSIONS

Based on the test results and analysis, it can be concluded that the steady-state operation current of the induction motor can be used as a parameter to detect the Broken Rotor Bar (BRB) fault. Empirical Mode Decomposition (EMD) analysis of the current signal is an alternative solution compared with other methods, such as the Fast Fourier Transform (FFT) analysis of the vibration signal, Continuous Wavelet Transform (CWT) analysis of the current signal, or sideband frequency analysis of the flux signal. EMD analysis was successfully applied as a signal processing technique to extract information from the current signal waveform. The EMD analysis resulted in the Intrinsic Mode Function (IMF 3) signal, which was used to obtain the Time Successive between Zero Crossing (TSZC) and Probability Density Function (PDF) shapes to distinguish between normal operation and fault severity. The shape parameters of the PDF, including the peak value, modus, and standard deviation, were used as input variables for the Artificial Neural Network (ANN) detection system.

Two ANN systems were designed for fault identification and severity detection. Based on the test results, the efficiency of the detection system was affected by the motor loading. A higher loading results in better performance of the detection system. Higher loading conditions resulted in an efficiency of 94.,89% and 76.09% for fault detection and severity identification, respectively. However, the ANN exhibited 88.04% efficiency and 71.89% severity identification for the lower loading category.

Based on the overall results, this method is proposed for induction motor diagnostics, particularly for rotor bar health assessment. The advantage of the proposed method is its ability to conduct an online assessment of the motor by only performing a very simple current measurement. Steady-state current measurements under higher loading conditions are applicable in industry. Moreover, to improve the detection performance, the detection system must be trained with more cases and measurements.

## ACKNOWLEDGMENT

The authors gratefully acknowledge the Institut Teknologi Sepuluh Nopember for the financial support of this work under the project scheme of the Publication Writing and IPR Incentive Program (PPHKI) 2022 for the data processing of this research.

## DATA AVAILABILITY

The authors confirm that the supporting data are available upon request.

## REFERENCES

[1] R. Valles-Novo, J. de Jesus Rangel-Magdaleno, J. M. Ramirez-Cortes, H. Peregrina-Barreto, and R. Morales-Caporal, "Empirical Mode Decomposition Analysis for Broken-Bar Detection on Squirrel Cage Induction Motors," *IEEE Transactions on Instrumentation and Measurement*, vol. 64, no. 5, pp. 1118–1128, May 2015, https://doi.org/10.1109/TIM.2014.2373513.

[2] A. Allal *et al.*, "Advanced Residual Optimal Mapping Approach for Precise Detection of Stator Faults in Induction Motors," *IEEE Access*, vol. 12, pp. 143515–143530, 2024, https://doi.org/10.1109/ACCESS.2024.3442671.

[3] M.-Q. Tran, M.-K. Liu, Q.-V. Tran, and T.-K. Nguyen, "Effective Fault Diagnosis Based on Wavelet and Convolutional Attention Neural Network for Induction Motors," *IEEE Transactions on Instrumentation and Measurement*, vol. 71, 2022, Art. no. 3501613, https://doi.org/10.1109/TIM.2021.3139706.

[4] C. S. Kalaskar and V. J. Gond, "Motor Current Signature Analysis to Detect the Fault in Induction Motor," *Int. Journal of Engineering Research and Applications*, vol. 4, no. 6, pp. 58–61, 2014.

[5] M. Bachir Bechiri *et al.*, "Effective Diagnosis Approach for Broken Rotor Bar Fault Using Bayesian-Based Optimization of Machine Learning Hyperparameters," *IEEE Access*, vol. 12, pp. 139923–139936, 2024, https://doi.org/10.1109/ACCESS.2024.3464108.

[6] K. Drobnič, M. Nemec, H. Lavrič, V. Ambrožič, and R. Fišer, "Detection of Broken Rotor Bars in Presence of Load Oscillations," *IEEE Access*, vol. 13, pp. 40012–40027, 2025, https://doi.org/10.1109/ACCESS.2025.3546705.

[7] G. Liu *et al.*, "A Double-Branch Improved Residual Shrinkage Network for Diagnosis of Induction Motor Broken Rotor Bar Under Small Samples," *IEEE Transactions on Instrumentation and Measurement*, vol. 74, 2025, Art. no. 3502012, https://doi.org/10.1109/TIM.2024.3502726.

[8] B. Battulga, M. Faizan Shaikh, J. Wook Chun, S. Bong Park, S. Shim, and S. B. Lee, "MEMS Accelerometer and Hall Sensor-Based Identification of Electrical and Mechanical Defects in Induction Motors and Driven Systems," *IEEE Sensors Journal*, vol. 24, no. 19, pp. 31104–31113, Oct. 2024, https://doi.org/10.1109/JSEN.2024.3447869.

[9] P. Wang, K. Wang, and L. Chen, "Broken Rotor Bars Detection in Inverter-Fed Induction Motors Under Continuous Switching of Different Speed Modes," *IEEE Transactions on Industrial Electronics*, vol. 71, no. 1, pp. 975–984, Jan. 2024, https://doi.org/10.1109/TIE.2022.3225851.

[10] G. Niu, X. Dong, and Y. Chen, "Motor Fault Diagnostics Based on Current Signatures: A Review," *IEEE Transactions on Instrumentation and Measurement*, vol. 72, 2023, Art. no. 3520919, https://doi.org/10.1109/TIM.2023.3285999.

[11] D. Pasqualotto and M. Zigliotto, "Increasing Feasibility of Neural Network-Based Early Fault Detection in Induction Motor Drives," *IEEE Journal of Emerging and Selected Topics in Power Electronics*, vol. 10, no. 2, pp. 2042–2051, Apr. 2022, https://doi.org/10.1109/JESTPE.2021.3115170.

[12] X. Hou, F. Du, K. Huang, J. Qiu, and X. Zhong, "A Current-Based Fault Diagnosis Method for Rotating Machinery With Limited Training Samples," *IEEE Transactions on Instrumentation and Measurement*, vol. 72, 2023, Art. no. 3530414, https://doi.org/10.1109/TIM.2023.3314809.

[13] S. Xue *et al.*, "Induction Motor Failure Identification Based on Multiscale Acoustic Entropy Feature Selection and Hierarchical Adaptive Neuro-Fuzzy Inference System With Localized Recurrent Input," *IEEE Sensors Journal*, vol. 23, no. 24, pp. 30821–30834, Dec. 2023, https://doi.org/10.1109/JSEN.2023.3329770.

[14] A. F. Khalil and S. Rostam, "Machine Learning-based Predictive Maintenance for Fault Detection in Rotating Machinery: A Case Study," *Engineering, Technology & Applied Science Research*, vol. 14, no. 2, pp. 13181–13189, Apr. 2024, https://doi.org/10.48084/etasr.6813.

[15] J. Shin, Y. Park, and S. B. Lee, "Flux-Based Detection and Classification of Induction Motor Eccentricity, Rotor Cage, and Load Defects," *IEEE Transactions on Industry Applications*, vol. 57, no. 3, pp. 2471–2480, May 2021, https://doi.org/10.1109/TIA.2021.3066960.

[16] C.-Y. Lee and E. D. C. Maceren, "Induction motor bearing fault classification using deep neural network with particle swarm optimization-extreme gradient boosting," *IET Electric Power Applications*, vol. 18, no. 3, pp. 297–311, Mar. 2024, https://doi.org/10.1049/elp2.12389.

[17] D. Matić, F. Kulić, V. Climente-Alarcón, and R. Puche-Panadero, "Artificial neural networks broken rotor bars induction motor fault detection," in *10th Symposium on Neural Network Applications in Electrical Engineering*, Belgrade, Serbia, Sep. 2010, pp. 49–53, https://doi.org/10.1109/NEUREL.2010.5644051.

[18] G. Zhang, B. Eddy Patuwo, and M. Y. Hu, "Forecasting with artificial neural networks:: The state of the art," *International Journal of Forecasting*, vol. 14, no. 1, pp. 35–62, Mar. 1998, https://doi.org/10.1016/S0169-2070(97)00044-7.

[19] J. Zhang, G. G. Walter, Y. Miao, and W. N. W. Lee, "Wavelet neural networks for function learning," *IEEE Transactions on Signal Processing*, vol. 43, no. 6, pp. 1485–1497, Jun. 1995, https://doi.org/10.1109/78.388860.

[20] S. Zolfaghari, S. B. M. Noor, M. Rezazadeh Mehrjou, M. H. Marhaban, and N. Mariun, "Broken Rotor Bar Fault Detection and Classification Using Wavelet Packet Signature Analysis Based on Fourier Transform and Multi-Layer Perceptron Neural Network," *Applied Sciences*, vol. 8, no. 1, Jan. 2018, Art. no. 25, https://doi.org/10.3390/app8010025.